J. Fluid Mech. (1983), *vol.* 136, *pp.* 375–391
Printed in Great Britain

On critical flow around smooth circular cylinders

By C. FARELL

St Anthony Falls Hydraulic Laboratory, Department of Civil and Mineral Engineering, University of Minnesota, Minneapolis, Minnesota 55414

AND J. BLESSMANN

Laboratório de Aerodinâmica das Construcões, Pós-Graduação em Engenharia Civil, Universidade Federal do Rio Grande do Sul, Porto Alegre, Brasil

(Received 5 April 1983)

The characteristics of the flow around a smooth circular cylinder in the critical Reynolds-number range have been investigated experimentally on the basis of instantaneous mean-pressure-distribution measurements on the cylinder and of hot-wire velocity-fluctuation measurements in the cylinder wake. Two subregions have been identified in the critical or lower transition; the first characterized by symmetric pressure distributions, intense vortex shedding, and gradual and significant variations in characteristic parameters as the Reynolds number increases, and the second by intense flow oscillations associated with formation and bursting of laminar-separation bubbles on one or both sides of the cylinder, without preference for side. The spectra of the velocity fluctuations in the second, unsteady subrange appear in general with broad band peaks. The spectral peak in the twin-bubble regime which follows this second subrange is sharp but has little energy compared to subcritical peaks.

1. Introduction

The flow around a nominally smooth circular cylinder at Reynolds numbers larger than, say, 5×10^4, is characterized by the occurrence of transitional changes separating flow regimes with basically different boundary-layer behaviours. As first suggested essentially by Roshko (1961), at least three regimes can be identified: subcritical (purely laminar boundary-layer separation), supercritical (laminar separation followed by turbulent reattachment and eventual turbulent separation), and transcritical (transition to turbulence in the boundary layer occurring ahead of separation). It is now firmly established (see e.g. Achenbach 1968; Bearman 1969) that the formation of laminar-separation–turbulent-reattachment bubbles is responsible for the low values of the drag coefficient C_D which occur at the beginning of the supercritical regime. The lower or critical transition separating the subcritical and supercritical ranges is marked by a pronounced decrease in C_D, from about 1.15 at $Re \approx 1.5 \times 10^5$ to about 0.25 at $Re \approx 4 \times 10^5$. The actual values vary for different experimental set-ups, since the flow characteristics in the transition range are rather sensitive to factors such as freestream turbulence and model geometry, including wind-tunnel blockage, model end conditions and alignment, length-to-diameter ratio, and possible surface irregularities which may disturb the thin boundary layers ahead of separation.

Existing measurements, although relatively numerous, are still not completely unambiguous with regard to the physical mechanisms underlying both the lower (subcritical–supercritical) and upper (supercritical–transcritical) transitions. The

comparatively recent nature of developments concerning the existence of the laminar separation bubbles, the difficulty of conducting experiments at sufficiently large Re, and inherent difficulties in the experimental measurements themselves can be cited as contributing factors to this state of affairs. As a result, somewhat conflicting interpretations of the flow phenomena have appeared, including a confusing use of terminology (the authors' included) to designate the recently recognized flow regimes.

The the authors' knowledge, the only detailed experimental investigation of the sequence of events taking place at the lower transition as Re increases from subcritical to supercritical is that of Bearman (1969), who reported in particular the presence of a single asymmetric bubble, always on the same side of the cylinder, over a subrange of Re before symmetric twin bubbles appeared. The present paper presents additional experimental results over this lower transition, where C_D exhibits such a pronounced decrease, to illustrate the nature of the flow and characterize certain subregimes which can be identified. The experimental measurements, which incidentally were obtained under a tight schedule and were prompted by a somewhat fortuitous observation of the flow while conducting a related investigation, include instantaneous mean-pressure-distribution measurements and hot-wire velocity-fluctuation measurements at various positions in the cylinder wake. The question of flow-regime terminology is also discussed.

2. Experimental arrangement and procedure

The experiments were carried out in the TV-2 wind tunnel of the Universidade Federal do Rio Grande do Sul (Blessmann 1982). The test section is 9.32 m long, with a height of 0.90 m and a width of 1.24 m at the test section where the model was located. The cylinder model had a diameter of $d = 0.147$ m and spanned the height of the tunnel, without endplates, giving a length-to-diameter ratio $L/d = 6.14$. It was turned out of a steel pipe and its surface was left in the as-machined condition. The base of the cylinder was attached to a rotating steel table, supported externally on a tripod on a concrete base, which is part of the wind-tunnel floor but is structurally independent of the tunnel frame. The top of the cylinder was attached to a heavily weighted and stayed external portico through a Gimball ball bearing, which could absorb any misalignment but provided a tight fit to reduce cylinder vibrations as much as possible. The vibrations of the cylinder were measured to ensure the adequacy of the set-up. The displacements Δ of the cylinder at its midsection for a 37 m/s wind were as follows:

$$\begin{aligned} \text{in the longitudinal direction} \quad & \Delta_{\text{rms}} = 0.007 \text{ mm}, \\ & \Delta_{\text{peak}} = 0.016 \text{ mm}; \\ \text{in the transverse direction} \quad & \Delta_{\text{rms}} = 0.024 \text{ mm}, \\ & \Delta_{\text{peak}} = 0.050 \text{ mm}. \end{aligned}$$

The natural frequency of the cylinder supported as described was 46 Hz.

The TV-2 tunnel freestream turbulence intensity $(\overline{u'^2})^{\frac{1}{2}}/U$, where u' is the longitudinal velocity fluctuation and U is the wind mean velocity, is 0.4 % for $U = 40.5$ m/s. Under the same conditions, the integral scale of the longitudinal velocity fluctuations is about 0.01 m.

Mean-pressure distributions were obtained by means of 28 pressure taps on the cylinder midsection. The angular location of the taps can be seen in figures 1–5, which

show the measured values of the mean-pressure coefficients, $C_p = (\bar{p}-p_0)/\frac{1}{2}\rho U^2$, where $\bar{p}$ is the mean pressure at angular location θ, p_0 is the undisturbed stream static pressure, and ρ is the mass density of the fluid, as functions of θ. Additional taps at $\theta = 0$, $\pm 70°$ and $\pm 60°$, on transverse sections two diameters above and below the cylinder midsection, were used also for the mean-pressure measurements. The mean-pressure tubes were connected to an alcohol multimanometer, so that a simultaneous display of all the measured pressures was available at all times. The C_p coefficients were calculated from instantaneous photographs of the multimanometer deflections. Micromanometer checks of the values read from print blow-ups were made to ensure the accuracy of the procedure. The symmetry of the pressure distributions measured outside the transition region confirmed the uniformity of the tunnel flow, the correct vertical alignment of the cylinder, and the correct location of the pressure taps.

A TSI hot-film anemometer, model 1054A, was used to obtain the velocity fluctuation data. The sensor was placed 0.23 m behind the cylinder axis, in four different lateral positions with respect to the tunnel centreplane:

position 1, 83 mm to the left (looking downstream);

position 2, 73 mm to the right;

position 3, 29 mm to the right;

position 4, on the tunnel centreplane.

The anemometer signals were recorded on magnetic tape using a Hewlett-Packard four-channel FM tape recorder, model 3960. The spectral analysis was done analogically with a Bruel & Kjaer spectral analyser, model 2120-A.

3. Presentation of results

3.1. *Mean-pressure measurements*

Figures 1–5 show representative mean-pressure distributions over the Re-range investigated, as obtained from the photographic records of the simultaneous multimanometer deflections. With increasing Re, above 3×10^5, large oscillations were observed in these distributions. While oscillating, the pressure distributions (and the flow) would remain relatively steady at times for a few seconds, and then all pressures would change in unison to a different configuration. Symmetric and asymmetric configurations were possible for the same Re. In general, for $Re < 3 \times 10^5$, symmetric distributions were obtained, as shown in figure 1, with gradual changes in the C_p values. These distributions were roughly similar to the subcritical pressure distributions (say, $Re < 1.5 \times 10^5$), with minimum pressure coefficients C_{pm} relatively small in absolute value, and base-pressure coefficients C_{pb} indicating relatively large wake suctions (see also figures 12 and 13). As Re increased towards 3×10^5, however, these symmetric distributions developed an inflexion around $\theta = 90°$, and a lack of flow uniformity along the cylinder span began to be noticeable (see figure 1). Unfortunately, no time was available to investigate further the position of separation, which appeared to shift downstream as Re approached 3×10^5, but which may not be well defined by a C_p plot alone even if more pressure taps are used, requiring more elaborate techniques for accurate detection.

For Re greater than about 3×10^5, asymmetric distributions were observed, of the type shown in figures 2, 3 and 4. Each sample distribution in these figures consists of two halves: $\theta > 0$ and $\theta < 0$, corresponding to a single instantaneous photograph, and depicting conditions that prevailed for at least a few seconds. For $Re = 374000$,

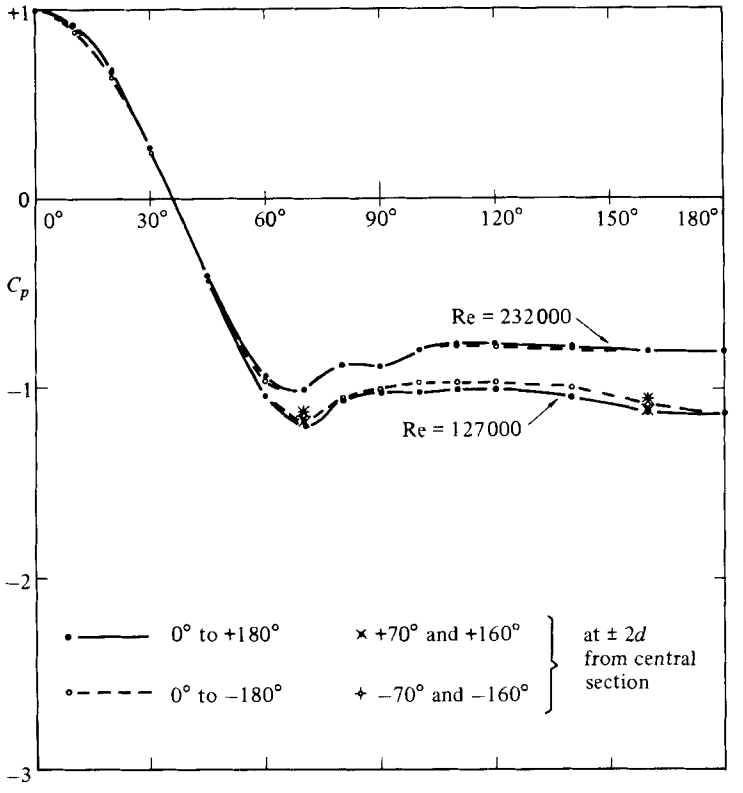

FIGURE 1. Pressure coefficient C_p as a function of circumferential angle θ (uncorrected for blockage). $Re = 1.27 \times 10^5$ and $Re = 2.32 \times 10^5$. (The data points for both Re at distances $\pm 2d$ from the centre section were almost coincident and only the points for $Re = 2.32 \times 10^5$ are shown.)

for example, two sample distributions are shown, one practically symmetrical and uniform along the cylinder span, the other asymmetrical and exhibiting a large non-uniformity along the span. For all Reynolds numbers investigated, the asymmetry occurred without preference for one or the other side of the cylinder. The maximum suctions would occur for $\theta < 0$ as in figure 4, sample 1, and would then change to the opposite side, or a symmetric configuration would occur as in sample 2 of figure 4, without a change in Re. (The wind-tunnel speed did not change appreciably with these flow oscillations, very likely due to the energy losses in the tunnel, in addition to that introduced by the cylinder, and to the fan and flow control used.) Figure 3 shows six sample distributions for a smaller Re, with maximum suctions occurring on one or the other side of the cylinder. For $Re > 3.8 \times 10^5$, the distributions became stable, symmetrical, and uniform along the cylinder span, exhibiting large side suctions, as depicted in figure 5 for $Re = 3.8 \times 10^5$.

Also shown in figure 5 is the correction for wall interference as applied to the distribution for $Re = 3.8 \times 10^5$, to illustrate the magnitude of the corrections incorporated in figures 12, 13 and 14. The method used is discussed at length in Farell *et al.* (1977), and is essentially that developed by Allen and Vincenti, with a modification for consistency which results only in small changes for moderate blockages. Strictly speaking, this method can be applied at best only in a qualitative manner in the critical Reynolds-number range. The flow parameters vary rapidly in this range with changes in Re, and the interference of the walls may result in shifts in the occurrence

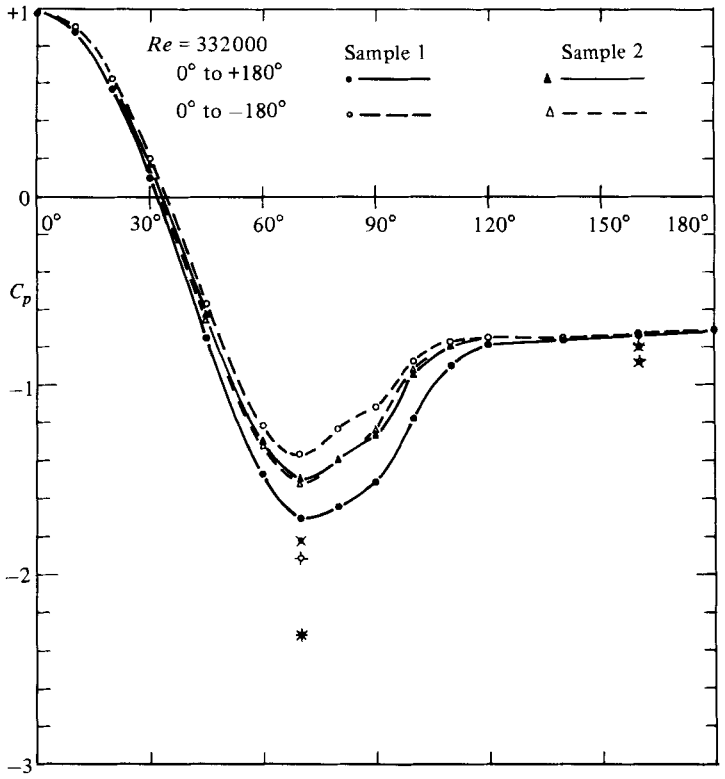

FIGURE 2. Pressure coefficient C_p as a function of circumferential angle θ (uncorrected for blockage). $Re = 3.32 \times 10^5$, two sample distributions, Other symbols as in figure 1.

of the transition phenomena which are responsible for the variations. The results of Richter & Naudascher (1976) tend to indicate that these shifts, and the effects of wall confinement on peak Strouhal numbers, are small for blockage ratios less than, say, 10 %. No correction has been applied here to Strouhal-number values.

3.2. *Spectral-density measurements of velocity fluctuations*

Figures 6–9 show the spectra (divided by the variance σ^2 of the fluctuations) of the hot-wire anemometer signals, with the probe positioned at various points in the wake as indicated in figure 6. This figure shows also the spectrum for $Re = 127000$ over three decades of Strouhal number $S = fd/U$ as a reference for comparison. There is strong vortex shedding and a clearly defined peak containing the major part of the total energy. Smaller peaks corresponding to the second and third harmonics of the vortex-shedding frequency can also be observed. (Neither of these two peaks coincide with the cylinder's natural frequency, 46 Hz.)

Figures 7, 8 and 9 show the progression of spectral changes that occur as Re increases. For Re less than about 3×10^5, with symmetric pressure distributions (figure 1), strong shedding persisted as Re increased, but with smaller spectral peaks. For $Re = 332000$, with oscillating and asymmetric pressure distributions (see figure 2, the oscillations were still limited for this Re), the spectral maxima are an order of magnitude smaller than the peak maximum for $Re = 127000$. As the Reynolds number and the asymmetry and oscillations of the mean pressure distributions became larger, the peak densities decreased further. For $Re = 348000$ (figure 9*a*) the

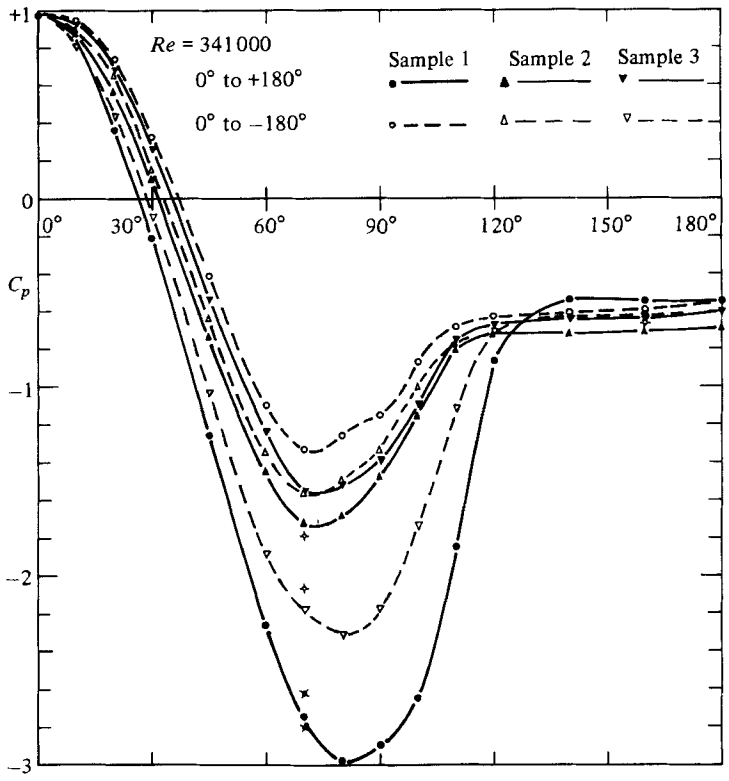

FIGURE 3. Pressure coefficient C_p as a function of circumferential angle θ (uncorrected for blockage). $Re = 3.41 \times 10^5$, three sample distributions. Other symbols as in figure 1.

maximum is about 50 times smaller than that for $Re = 127000$. Although the location of the probe affected somewhat the shape of the spectral density functions, the peak levels for positions 1, 2 and 3 investigated were about the same within the experimental error. (The spectral densities depend generally on the probe position in the wake. Relative peak energy levels and peak Strouhal numbers are used herein to characterize flow regimes and transition phenomena, in particular the onset of 3-dimensional flow.) Figure 9(*b*) corresponds to position 4 on the flow centreline; the Strouhal number for the relatively sharp (but rather reduced) peak is 0.849, exactly double the value corresponding to the peak in figure 9(*c*), 0.424. The latter figure shows the spectrum that results as the flow oscillations cease and the steady mean pressure distribution of figure 5, with large C_{pm} values, is obtained. The peak in figure 9(*c*) is still 50 times smaller than that for $Re = 127000$.

Figures 10 and 11 illustrate the hot-wire signals for several Reynolds numbers. The traces in figure 10 depict the regularity of the subcritical shedding signals and the progressive deterioriation of organized shedding as Re increases. For $Re = 232000$ (figure 10*c*) the C_p distributions (figure 1) were symmetric, but showed already appreciable non-uniformity along the cylinder span; the spectral peak (figure 7*c*) was sharp but three times smaller than the peak for $Re = 127000$. As Re was increased further and the flow oscillations appeared, the shedding became non-stationary, resulting in broadband peaks. The various shedding components did not all occur simultaneously, however, as figures 11(*b*, *c*) suggest (see §4). For $Re = 332000$ (figure 11*a*), with (relatively small) oscillations of the C_p distributions of the order illustrated

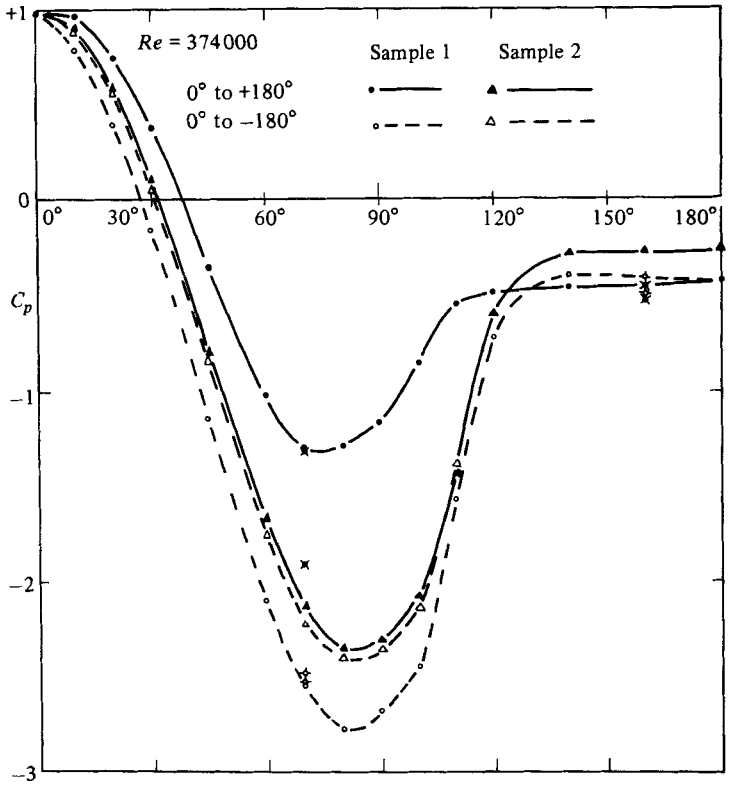

FIGURE 4. Pressure coefficient C_p as a function of circumferential angle θ (uncorrected for blockage). $Re = 3.74 \times 10^5$, two sample distributions. Other symbols as in figure 1.

in figure 2, the shedding appeared to produce two peaks (figure 8*a*), one at $S = 0.176$ which follows the trend depicted in figure 7 of decreasing S-values with increasing Re, the other at a larger $S \approx 0.20$, corresponding to a narrower wake. As Re increased, the lower Strouhal number components of the shedding diminished in magnitude and higher-Strouhal-number components appeared and eventually replaced them (see figures 8 and 9*a*). For $Re = 374000$ it appears from figure 9(*b*) that most of the shedding takes place in the two-bubble configuration (sample 2, figure 4). For $Re = 344000$, on the other hand, the relatively sharp spectral peak indicates that most of the shedding is predominantly in the single-bubble regime, with the bubble oscillating from one side of the cylinder to the other and the stationary probe falling alternately in and out of the cylinder wake, as the traces in figure 11 (*b*, *c*) suggest.

The smallness of the spectral peaks for all $Re > 3 \times 10^5$ investigated, in relation to the subcritical spectral peaks, should be noted.

3.3. *Characteristic flow parameters*

Figures 12, 13 and 14 show the minimum and base-pressure coefficients, C_{pm} and C_{pb}, measured on both sides of the cylinder, and the drag coefficient C_d, obtained by integration of the pressure distributions, as functions of Re. The base pressure coefficient is defined here as the average of the wake values excluding $\theta = 180°$. For the oscillating C_p distributions ($Re > 3 \times 10^5$) all $\theta > 0$ and $\theta < 0$ values measured for each Re are shown, representing asymmetric quasi-steady conditions which

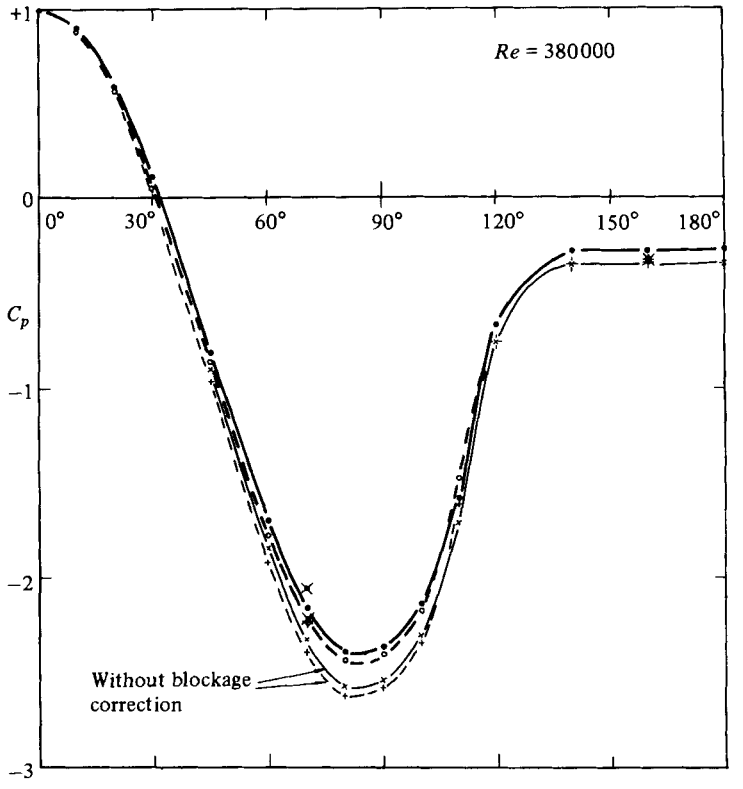

FIGURE 5. Pressure coefficient C_p as a function of circumferential angle θ for $Re = 3.8 \times 10^5$, with and without blockage correction. Other symbols as in figure 1.

obtained for each Re for a few seconds, resulting obviously in a multivalued functional relation. For $Re \geqslant 3.8 \times 10^5$, steady C_p distributions resulted, as shown in figure 5 for $Re = 3.8 \times 10^5$. The largest Re that could be achieved with the present set-up was slightly higher than 3.8×10^5, and no changes in the distributions were noted for these higher Reynolds numbers. This is indicated in the three figures with a short trace reaching past $Re = 4 \times 10^5$.

Figure 15 shows the peak Strouhal numbers measured concurrently with several of the pressure distributions presented earlier. The data of Bearman (1969) are also shown. Finally, table 1 gives the standard deviation σ of the velocity fluctuations, divided by U, for the Reynolds numbers of figures 7–9. These results are discussed in § 4. Calculation of the steady lift coefficient for the asymmetric pressure distributions gave values of the order of 1.0; the total force coefficient in the unsteady subrange was about 1.2.

4. Discussion

4.1. *Flow characteristics and regimes*

It has been customary in the literature to denote with the word critical the range of Reynolds numbers over which the pronounced decrease in C_d takes place. Single critical Reynolds numbers have also been defined, for example, as that Re at which C_d reaches its minimum after the abrupt decrease, or as the Re at which the jump in Strouhal number (to a value between 0.40 and 0.45) occurs. Leaving aside for the

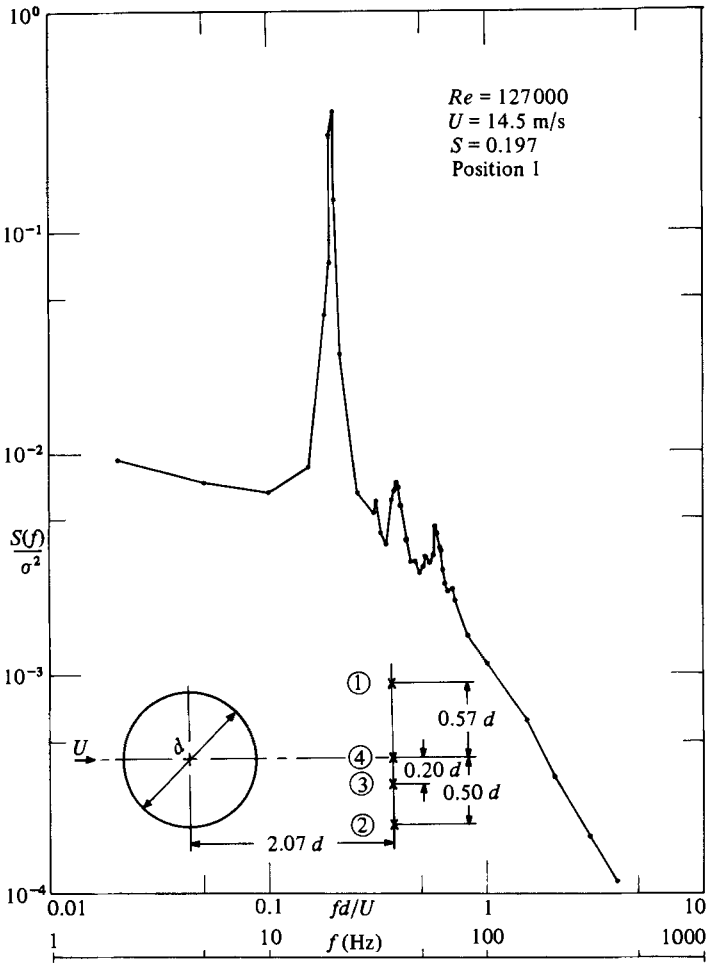

FIGURE 6. Spectral density of velocity fluctuations at position 1 for $Re = 1.27 \times 10^5$ and definition sketch of hot-wire positions.

moment the definition of a single critical Re, we discuss the characterization of the critical or lower transition as defined above. The limiting Reynolds numbers for the flow regimes described in the following are specific to the present experiments. Variations may be encountered for different experimental set-ups, for the reasons briefly outlined in the introduction. The close agreement with some of Bearman's (1969) limiting values, however, is noteworthy given the differences in cylinder finish and freestream turbulence level. (Bearman used a coated and highly polished cylinder in a tunnel with freestream turbulence level at 61 m/s equal to about 0.2%.)

As Re increased beyond about 1.5×10^5 (taken here as the end of the subcritical range) relatively gradual but pronounced changes occurred at first in the various flow parameters. The C_p distributions remained symmetric and steady during this initial transitional phase, but became appreciably non-uniform over the cylinder span. Between $Re = 1.5 \times 10^5$ and $Re = 3 \times 10^5$ approximately the following decreases were observed: C_d from 1.15 to 0.75, $|C_{pb}|$ from 1.05 to 0.60, $|C_{pm}|$ from 1.25 to 0.90 (note that $|C_{pm}|$ actually decreased over this Re-range). Concurrently, the spectral peaks of the wake velocity fluctuations, while remaining sharply defined and significant in

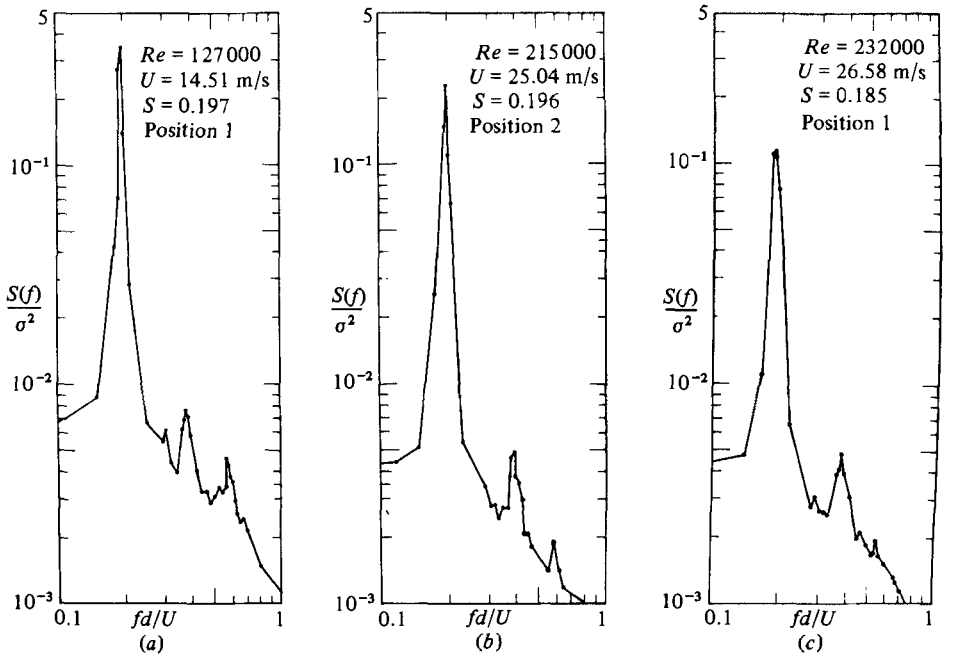

FIGURE 7. Spectral densities of velocity fluctuations for increasing values of Re. Symmetric pressure distributions. Probe positions as defined in figure 6.

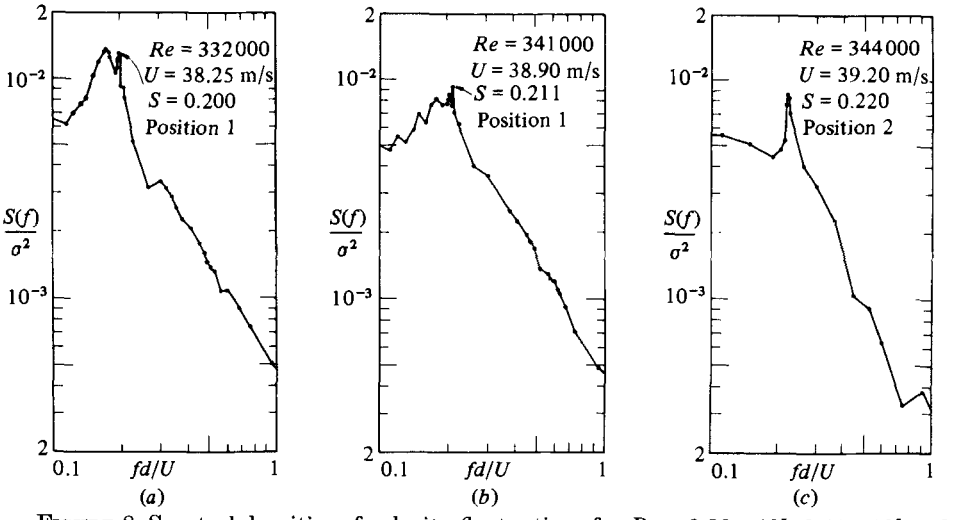

FIGURE 8. Spectral densities of velocity fluctuations for $Re = 3.32 \times 10^5$, 3.41×10^5 and 3.44×10^5. Probe positions as defined in figure 6.

terms of the signal variance in this first phase of the transition, decreased in magnitude (by a factor of three in figure 7). This decrease in the strength of the shedding is related to the increasing three-dimensionality of the flow along the cylinder span. Three-dimensional effects are responsible for the disappearance of narrowband organized shedding in the supercritical range of Reynolds numbers (see §4.2; a review of these effects can be found in Farell 1981). The disappearance results from the breakdown of the double-shear-layer interaction instability responsible for

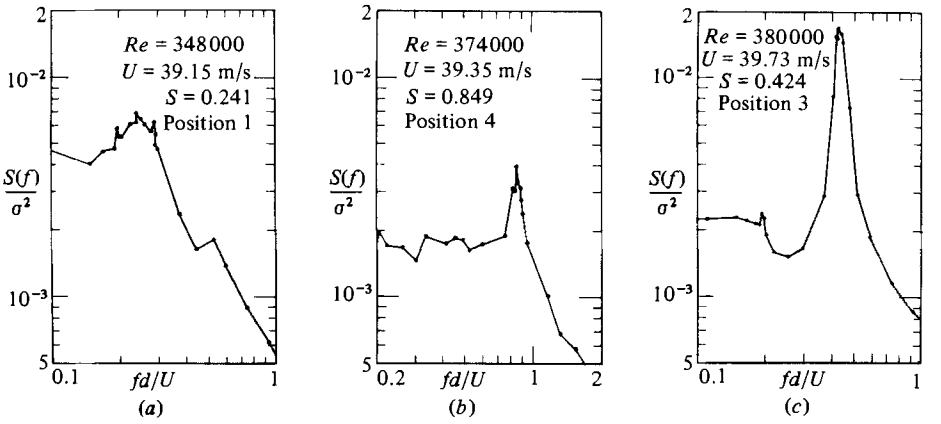

FIGURE 9. Spectral densities of velocity fluctuations for $Re = 3.48 \times 10^5$, 3.74×10^5 and 3.8×10^5. Probe positions as defined in figure 6.

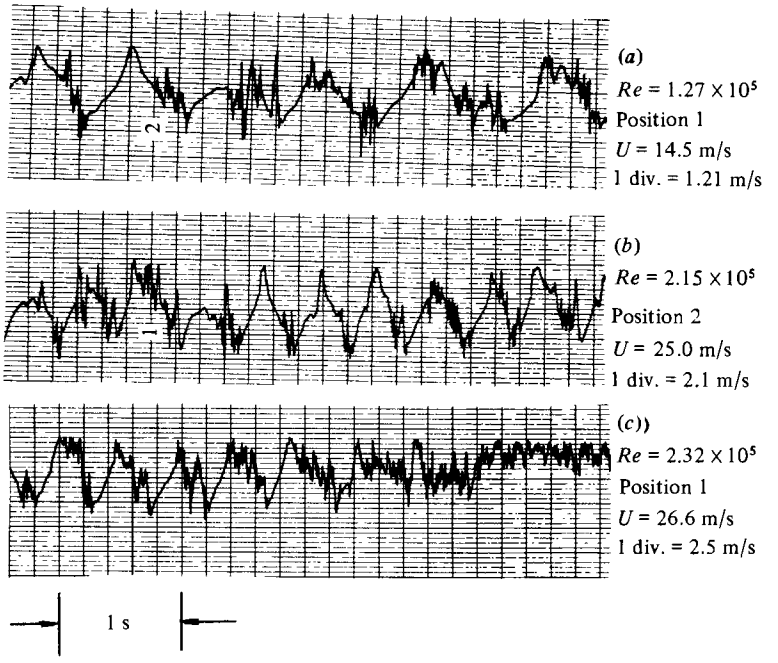

FIGURE 10. Anemometer traces. Subcritical and first subrange.

the shedding, brought about by the lack of spanwise uniformity. The present results show that in this phase of the transition the breakdown is fragmentary as one would expect (see figure 10*c*), but the effectiveness of the double-layer interaction and the shedding strength are gradually and significantly diminished. Partial reattachment of the separated shear layers could occur in this initial phase; secondary vortices due to single-layer instability could supply the necessary lateral momentum transfer for reattachment, forming perhaps a pulsating, long laminar bubble as suggested by Morkovin (1964).

The second phase of the transition began at $Re > 3 \times 10^5$, in a relatively gradual manner as one would expect from the nature of the shear-layer reattachment process.

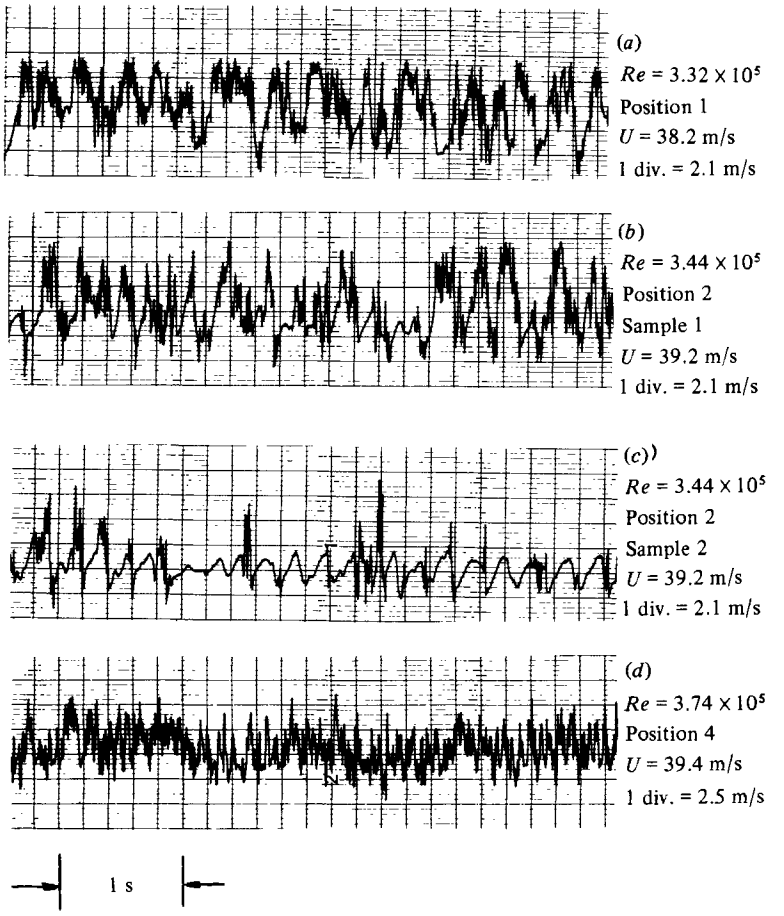

FIGURE 11. Anemometer traces. Single-bubble unsteady subrange.

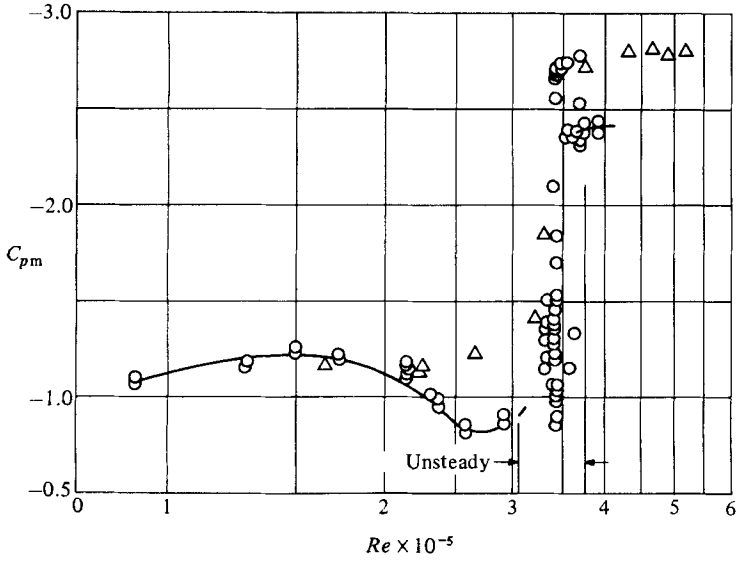

FIGURE 12. Minimum-pressure coefficient as a function of the Reynolds number (corrected for blockage): ○, present results; △, Güven *et al.* (1980).

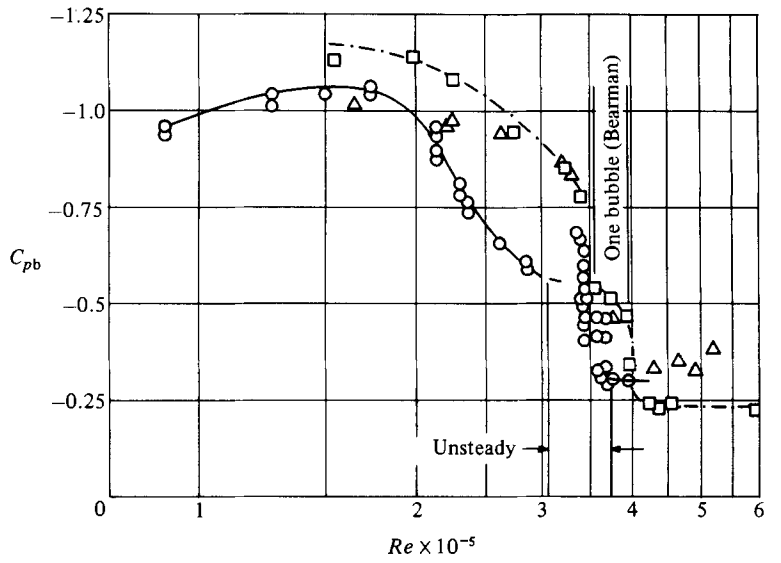

FIGURE 13. Base-pressure coefficient as a function of the Reynolds number (corrected for blockage): ○, present results; △, Güven *et al.* (1980); □, Bearman (1969).

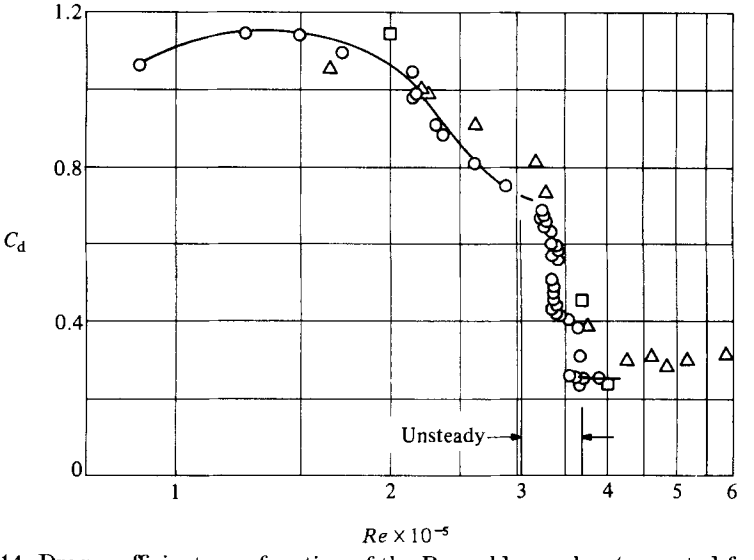

FIGURE 14. Drag coefficient as a function of the Reynolds number (corrected for blockage): ○, present results; △, Güven *et al.* (1980); □, Bearman (1969).

It was marked by the pronounced unsteadiness in the flow described earlier. The $|C_{pm}|$ values, in particular, showed rather large increases and oscillations (see figure 12), while the spectral maxima of the velocity fluctuations were at least an order of magnitude smaller than the subcritical peaks. The asymmetry and oscillatory behaviour of the flow in this subrange of the transition are attributed to the formation of a (short) laminar-separation–turbulent-reattachment bubble on one side of the cylinder only. Contrary to the results of Bearman (1969), who found the single-bubble regime to occur always with the bubble consistently on the same side of the cylinder,

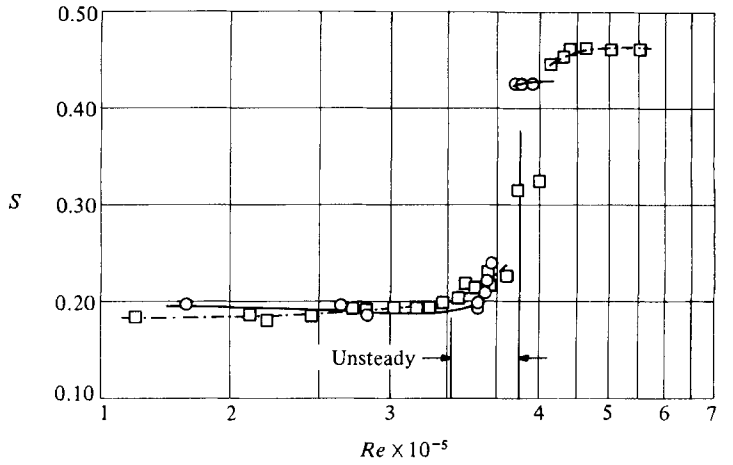

FIGURE 15. Strouhal number as a function of the Reynolds number (uncorrected for blockage): ○, present results; □, Bearman (1969).

$Re \times 10^{-5}$	1.27	2.15	2.32	3.32	3.41	3.48	3.74	3.80
σ/U	0.32	0.32 0.326	0.323	0.303 0.298	0.289	0.285	0.210	0.189

TABLE 1. Root mean square of velocity fluctuations

in the present experiments no preference was detected for the bubble to form on either side of the cylinder. (Some runs were repeated on different days to confirm this result which, to the authors' knowledge, has not been reported in the literature.) The alternating turbulent reattachment of the cylinder boundary layer (and eventual turbulent separation at a larger angle θ) was confirmed by the traces of the hot-wire signals, as illustrated in figures 11 (b, c). Bearman had already noted in his investigation that unsteady bubble formation and bursting (on the same side of the cylinder in his case) occurred prior to the appearance of his single-bubble (steady) regime and resulted in a double peak in the velocity spectra. These two peaks did not actually coexist. Likewise, under the conditions of the present experiments, vortex shedding occurred under varying (quasi-steady) flow configurations, adding contributions to the overall spectrum at different Strouhal frequencies which did not all obtain simultaneously, thus resulting in broad spectral peaks or maxima. As Re increased, the shedding contributions moved to higher Strouhal numbers. No peaks at $S \approx 0.32$ corresponding to Bearman's single-bubble peaks were found, probably because of the unsteadiness of the present single-bubble regime. For $Re = 3.44 \times 10^5$ (at which Re the C_p distributions were of the type of sample 1 in figure 3, always alternating sides) a relatively sharp (but small energywise) peak occurred at $S = 0.22$. At still higher Re the peak became broader and contained contributions from shedding at higher S-numbers (figure 9a). The relatively sharp peak at $S = 0.424$, for $Re = 3.74 \times 10^5$, implies significant shedding for this Reynolds number in the twin-bubble flow configuration (sample 2, figure 4). The twin-bubble regime is thus attained (as the other subranges) in a relatively gradual manner, with symmetric and asymmetric flow conditions alternating over a narrow Re-range.

In summary, the second phase of the transition range appears as being dominated by unsteadiness, as illustrated in particular by the quasi-steady results plotted in figures 12, 13 and 14. The transitional changes in C_d or in the other parameters in this subrange, as depicted by the present data, appear equally sharp and comparable to the sharpness of the change in the Strouhal number. The variation in the Strouhal number shown in figure 15 is actually smoothed out because it has been determined on the basis of the overall spectrum. Oscillatory Strouhal-number changes analogous to those in C_{pm} and C_{pb} should be observable if an appropriate conditional sampling could be used to pick out separately the individual shedding components for the different flow patterns.

Since the presence of small roughnesses or other boundary-layer disturbances greatly affect the resulting unsteady flow patterns and their three-dimensional spanwise behaviour, long-term averages in the critical range will be strongly dependent on wind-tunnel and model conditions. Wall interference and end effects in particular may be substantial, and with present blockage-correction methods not strictly applicable in the critical range except at best in a rather qualitative manner, comparison of data from different sources becomes difficult. Long-term averaging, on the other hand, smoothes out the changes in the various parameters, and so does the integration of the two-sided pressure distributions to obtain C_d (see figure 14). A comparison with the data of Güven, Farell & Patel (1980) is presented in figures 12, 13 and 14. These data represent long-term averages and have been corrected for blockage. (Blockage and length-to-diameter ratios were respectively 17.8 % and 3.08, compared with 11.9 % and 6.14 % for the present experiments.) Despite the differences in the experimental set-ups, the C_d data can be considered in broad agreement. The same cannot be said of the minimum C_{pm} values, which show somewhat larger differences, likely due to the different blockage and length-to-diameter ratios. We note here that for $Re = 3.74 \times 10^5$, the $|C_{pm}|$ values for the symmetric pressure distribution of figure 4 are smaller than the larger of the two $|C_{pm}|$ values for the asymmetric distribution in the same figure. The $|C_{pm}|$ values in the two-bubble steady regime ($Re \geqslant 3.8 \times 10^5$) were actually smaller than some of the quasi-steady values measured for smaller Re in the single-bubble range.

The data of Bearman (1969) have also been added for comparison in figures 13, 14 and 15. The blockage ratio of these experiments was 6.5 % and the length-to-diameter ratio 12; the mean pressure at $\theta = 180°$ was used to define C_{pb}. Bearman's single-bubble steady regime falls slightly to the right of the present unsteady range. It should be noted, however, that $Re \approx 3.8 \times 10^5$ is given in the text of this reference as the Reynolds number at which the two-bubble regime materialized, which coincides with the Re at which this regime was first observed in the present experiments.

4.2. *Definitions and nomenclature*

In the twin-bubble range the present results show sharp but small spectral peaks (see figure 9*c*) with Strouhal numbers between 0.42 and 0.43, corresponding to a much narrower wake than in the subcritical range. The Strouhal number as first measured by Bearman in this range was 0.46. Since Reynolds numbers larger than about 4×10^5 could not be reached with the present set-up, the disappearance of narrow-band organized shedding at larger Re (say, $Re = 6 \times 10^5$) as described by Bearman and confirmed by numerous other measurements (e.g. Roshko 1961; Jones, Cincotta & Walker 1969; Batham 1973; additional references in Farell 1981) could not be observed. This disappearance is due to 3-dimensional effects as described earlier,

except that now turbulent spots arising in the laminar boundary layers ahead of the bubbles are responsible for the spanwise fragmentation of the bubbles and the breakup of the double-layer instability mechanism. The Reynolds number at which organized shedding eventually disappears is greatly dependent on disturbances in a rather general way. Achenbach & Heinecke (1981) have reported observing narrowband shedding peaks on one of their cylinder models ($L/d = 6.75$) up to $Re = 10^6$; no information is given on peak energy levels. For $Re > 10^6$, the measured fluctuation spectra were broad and determination of a single Strouhal number was subject to a large scatter band according to this reference. The scatter is also present in the Strouhal-number data of Delany & Sorensen (1953), which, as these authors indicate, represent 'predominant frequencies encountered'; spectral energy levels are not given. Incidentally, the breakup of the laminar separation bubbles in the supercritical range is well illustrated by the oilflow photographs of Jones *et al.* (1969), which show turbulent wedges locally wiping out the separation bubble and thereby changing the position of final turbulent separation.

Under the conditions described it seems convenient to define the upper limit of the critical range to coincide with the appearance at $Re = 3.8 \times 10^5$ of the two symmetric bubbles rather than with the later disappearance of organized shedding. With this definition, the twin-bubble range is included as part of the supercritical Re-range, at the beginning of which $|C_{pm}|$ and S reach their maxima and $|C_{pb}|$ and C_d their minima. Narrowband vortex shedding either would occur in the supercritical range with sharp spectral peaks and little energy, or it would not occur at all at sufficiently high Re. The name, lower transition, suggested by Roshko for the critical range seems appropriate to differentiate it from the upper transition, which marks the end of the supercritical range and the beginning of the post- or transcritical regime. The latter regime, incidentally, could perhaps be called ultracritical if this would help eliminate some of the confusion in the nomenclature presently used by different authors.

5. Conclusions

Two subregimes can be distinguished in the critical or lower transition. The first ($1.5 \times 10^5 < Re < 3 \times 10^5$) is characterized by symmetric pressure distributions, an increasing lack of uniformity along the cylinder span, and gradually varying characteristic parameters, among which C_d, $|C_{pm}|$ and $|C_{pb}|$ decrease substantially. The effectiveness of the double-layer interaction, and consequently the vortex-shedding strength, decrease in this subrange, although the shedding remains intense, with slightly diminishing Strouhal numbers. The second subregime is characterized by intense flow oscillations due to formation and bursting of a single bubble on one or the other side of the cylinder, at first intermittently on either side, then in an alternating fashion as Re increases, and finally alternating with a two-bubble flow pattern. The twin-bubble regime becomes steady with symmetric pressure distributions at $Re = 3.8 \times 10^5$. The spectra of wake velocity fluctuations in this unsteady subrange appear in general with broadband peaks as shedding under different flow configurations adds succeeding spectral components with different Strouhal numbers. Narrow but always weak peaks are possible if a single configuration predominates. The spectral peak in the twin-bubble regime is sharp but has little energy compared to a subcritical peak.

The critical range or lower transition can be defined as starting at $Re = 1.5 \times 10^5$, where C_d begins to fall, and ending at $Re = 3.8 \times 10^5$, were the steady twin-bubble flow forms. The transition between subregimes is relatively gradual and can be placed

as beginning at $Re \approx 3 \times 10^5$. The limiting Reynolds numbers given here must be considered specific to the present study, given the sensitivity of the flow characteristics in the transition range to factors such as freestream turbulence, model geometry and surface roughness. It is noted, however, that $Re = 3.8 \times 10^5$ is also given by Bearman (1969) as the Reynolds number at which the twin-bubble regime materialized.

The support of the National Science Foundation under Grants ENG 78-22092 and INT-800 8014, and of Conselho Nacional de Desenvolvimento Científico e Tecnológico, Brasil, is gratefully acknowledged.

REFERENCES

ACHENBACH, E. 1968 Distribution of local pressure skin friction around a circular cylinder in cross flow up to $Re = 5 \times 10^6$. *J. Fluid Mech.* **34**, 625–639.

ACHENBACH, E. & HEINECKE, E. 1981 On vortex shedding from smooth and rough cylinders in the range of Reynolds numbers from 6×10^3 to 5×10^6. *J. Fluid Mech.* **109**, 239–251.

BATHAM, J. P. 1973 Pressure distributions on circular cylinders at critical Reynolds numbers. *J. Fluid Mech.* **57**, 209–228.

BLESSMANN, J. 1982 The boundary-layer TV-2 wind tunnel of the UFRGS. *J. Wind Engng and Indust. Aerodyn.* **10**, 231–248.

BEARMAN, P. W. 1969 On vortex shedding from a circular cylinder in the critical Reynolds number regime. *J. Fluid Mech.* **37**, 577–585.

DELANY, N. K. & SORENSEN, N. E. 1953 Low-speed drag of cylinders of various shapes. *NACA Tech. Note* 3038.

FARELL, C. 1981 Flow around fixed circular cylinders: fluctuating loads. *J. Engng Mech. Div. ASCE* **107** (EM3).

FARELL, C., CARRASQUEL, S., GÜVEN, O. & PATEL, V. C. 1977 Effects of wind tunnel walls on the flow past circular cylinders and cooling tower models. *Trans. ASME* I: *J. Fluids Engng* **99**, 470–479.

GÜVEN, O., FARELL, C. & PATEL, V. C. 1980 Surface roughness effects on the mean flow past circular cylinders. *J. Fluid Mech.* **98**, 673–701.

JONES, G. W., CINCOTTA, J. J. & WALKER, R. W. 1969 Aerodynamic forces on a stationary and oscillating circular cylinder at high Reynolds numbers. *NASA TR* R-300.

MORKOVIN, M. V. 1964 Flow around a circular cylinder – a kaleidoscope of challenging fluid phenomena. In *Proc. ASME Symp. on Fully Separated Flows*, pp. 102–118.

RICHTER, A. & NAUDASCHER, E. 1976 Fluctuating forces on a rigid circular cylinder in confined flow. *J. Fluid Mech.* **78**, 561–576.

ROSHKO, A. 1961 Experiments on the flow past a circular cylinder at very high Reynolds number. *J. Fluid Mech.* **78**, 561–576.